assumed to be singlemode, with a step-index profile. The delay τ is expressed by [7]

$$\tau = \frac{1}{c}\frac{d\beta}{dk} = \frac{1}{c}\left[N_2 + (N_1 - N_2)\frac{d(vb)}{dv}\right] \quad (3)$$

where, β, N_1, N_2, and v are the propagation constant, the group refractive index of the core, the group refractive index of the cladding, and the normalised frequency, respectively. The value b is defined in eqn. 4:

$$b = \frac{(\beta/n_2k)^2 - 1}{(n_1/n_2)^2 - 1} \quad (4)$$

in which $k = 2\pi/\lambda$ and λ is the wavelength. Therefore, the skew S is obtained by

$$S = \frac{n_2}{c}\delta\left[r\Delta\frac{d(vb)}{dv}\right] = 48\delta\Delta_{eff} \quad [\text{ps/m}] \quad (5)$$

in which

$$r = N_2/n_2$$

$$\Delta_{eff} = r\Delta\frac{d(vb)}{dv} = r\Delta[2(1-H) - b] \quad (6)$$

$$H = P_{clad}/P = \exp[-2(a/\omega)^2] \quad (7)$$

H is the ratio of power in a cladding to the total power P, and eqn. 7 is obtained by using the Gaussian field approximation [7]. By knowing the two values, core radius a and mode field radius ω, H can then be calculated. For the other two values, b and r, eqns. 8 and 9 are appropriate.

$$b = 0.472 + 0.965(a/\omega - 0.850) \quad (8)$$

$$r = 1.010 \text{ for } \lambda = 1.3\ \mu\text{m and } r = 1.013 \text{ for } \lambda = 0.55\ \mu\text{m} \quad (9)$$

The error in calculating b in eqn. 8 < 2% for $v = 2.3 \pm 0.2$. The values shown in eqn. 9 for r are obtained using the Sellmeier equation for pure silica. Using eqns. 5 – 9, we can calculate the skew, the results of which are shown in Table 1. Table 1 shows that the calculated data are closer to the measured values. The remaining error is not fully understood and it may be due to several stress effects.

The measured time of flight differences shown in Table 2 indicate the temperature independence for fibres with different Δ values. Therefore, we confirm that skew is temperature independent for fibre with different fibre parameters in a uniform temperature environment.

Conclusion: The fibre parameter dependence of skew for singlemode fibres has been clarified, both experimentally and theoretically.

8 July 1996
Electronics Letters Online No: 19961192

N. Kashima and H. Iwata (*NTT Access Network Systems Laboratories, Tokai-Mura, Naka-Gun, Ibaraki-ken 319-11, Japan*)

References

1 TAKAI, A., KATO, T., YAMASHITA, S., HANATANI, S., MOTEGI, Y., ITO, K., ABE, H., and KODERA, H.: '200-Mb/s/ch 100m optical subsystem interconnections using 8-channel 1.3μm laser diode arrays and single-mode fibre array', *J. Lightwave Technol.*, 1994, **LT-12**, (2), pp. 260–270

2 LAI, V.A., and ROSENMAYER, T.: 'Time of flight and skew in fibre optic ribbon cables subjected to thermal stress'. Proc. Int. Wire & Cable Symp., 1995, pp. 497–501

3 IWATA, H., MATSUMOTO, M., ISHINO, Y., TOMITA, S., NAGASAWA, S., and TANIFUJI, T.: 'Field test results for per-connectorized cable with 16-fibre ribbons'. Proc. Int. Wire & Cable Symp., 1994, pp. 774–780

4 TATEDA, M., TANAKA, S., and SUGAWARA, Y.: 'Thermal characteristics of phase shift in jacketed optical fibres', *Appl. Opt.*, 1980, **19**, (5), pp. 770–773

5 TACHIKURA, M., and KASHIMA, N.: 'Fusion mass-splices for optical fibres using high-frequency discharge', *J. Lightwave Technol.*, 1984, **LT-2**, (1), pp. 25–31

6 SHIBATA, S.: 'Fiber glasses for 0.6–6μm band transmission'. PhD Thesis, Hokkaido University, 1982

7 KASHIMA, N.: 'Passive optical components for optical fiber transmission' (Artech House, 1995)

Stable and broadband Er-doped superfluorescent fibre sources using double-pass backward configuration

L.A. Wang and C.D. Chen

Indexing terms: Superradiance, Optical fibres, Fibre optic gyroscopes

Er-doped superfluorescent fibre sources (SFSs) pumped near 980 nm in double-pass backward configuration are characterised experimentally for the first time. By properly adjusting erbium doped fibre lengths, SFSs can have pump-power insensitive mean wavelength operations with broader linewidths and better pump efficiencies than those in the commonly adopted single-pass backward configuration.

Introduction: Diode pumped rare-earth doped superfluorescent fibre sources (SFSs) have emerged as highly stable broadband sources for navigation-grade fibre optical gyroscopes (FOGs). Such SFSs may use Nd or Er-doped fibres as gain media which emit spectra in different wavelength ranges [1 – 3]. Er-doped SFSs have gained much attention because they are less sensitive to radiation losses than their Nd counterparts. Among many Er-doped SFS configurations, the single-pass backward (SPB) configuration has been commonly adopted owing to the relative ease of its design, and its lack of danger of lasing [3, 4]. Conversely, when operating an SFS in a double-pass configuration, either backward or forward, there is a need to be cautious in order to prevent the SFS from lasing. To date, most reports on double-pass SFSs are mainly simulation works, related to the double-pass forward (DPF) configuration [3, 5]. Experimental results regarding the lasing threshold and the output power of an SFS in the double-pass backward (DPB) configuration have been shown using Nd-doped fibres [2]. However, to the best of our knowledge, no theoretical or experimental results have been reported on an Er-doped SFS in the DPB configuration.

Additionally, the accuracy of rotation detection using an FOG is determined by the stability of the scale factor, which in turn depends on the stability of the mean wavelength of its light source. The mean wavelength is temperature dependent, and has three contributing sources [3]: intrinsic thermal effect, temperature effect of pump wavelength, and temperature effect of pump power. The last effect can be expressed as $(\partial \bar{\lambda}_{source}/\partial P_{pump})\cdot(\partial P_{pump}/\partial T)$. The intrinsic thermal effect is typically < 10ppm/°C [3, 6], while the temperature dependence of the pump wavelength can be minimised by operating an Er-doped SFS closer to its peak absorption wavelength (e.g. near 980nm) [5, 6]. The feasibility of pump-power independent mean wavelength operation, i.e. $\partial \bar{\lambda}_{source}/\partial P_{pump} = 0$, depends on the type of configuration used. Such operation has been so far reported only for an SFS in the SPB configuration [4, 7], but not in the DPB configuration as demonstrated in this Letter.

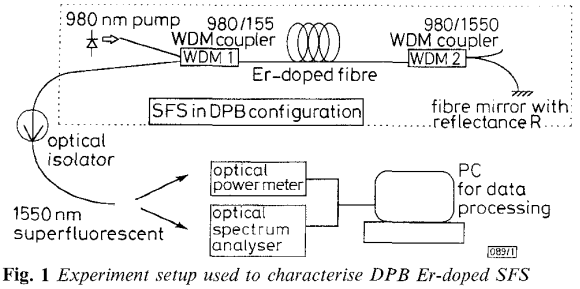

Fig. 1 *Experiment setup used to characterise DPB Er-doped SFS*

Experiment and discussion: The experimental setup used to characterise a DPB Er-doped SFS is shown as a schematic diagram in Fig. 1. Pump power was provided by a laser diode (Lasertron, Model QLM9S470-010) with the maximum output power of 82mW measured at the EDF input end. Two WDM couplers were used for the separation of pump and ASE signals. The doping concentration of the EDF was ~600wt ppm, and the EDF was singlemoded when pumped near 980nm. A fibre mirror with a

reflectance value of ~90% over the wavelength range of interest was spliced to the 1550 nm signal output end of the second WDM to reflect the forward ASE signal. To reduce optical feedback, a polarisation-insensitive isolator with ~59dB isolation (JDS VA5503-FPU) was incorporated at the output end of the SFS. The spectra and total output power of the SFS were measured and processed to calculate the mean wavelength [6], the linewidth [3] and the pumping efficiency.

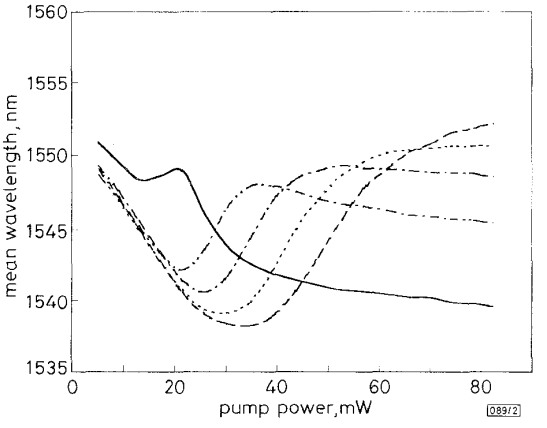

Fig. 2 *Mean wavelength against pump power*

– – – – 12m
- - - - - 11m
– · – · 10m
– ·· – ·· 9m
——— 7m

The variation of mean wavelength with a pump power of a DPB SFS for various EDF lengths was characterised, and the results are shown in Fig. 2. It was found that for longer EDF lengths (~>7m), there existed two regions where the mean wavelength had little or no dependence on pump power. These two regions corresponded to different pump power levels, and, as the lengths of EDFS increased, were found to have shifted towards higher pump-power sides. In addition, for a given EDF length, the mean wavelengths in high-pump (> 35mW) regions were much more stable than those in low-pump regions, owing to their slow slope variations resulting from the difference of spectral evolution along the EDF length. In high pump regions, the pump-power independent mean wavelength operation, i.e. where $\partial \bar{\lambda}_{source}/\partial P_{pump} = 0$, would always be obtained by properly adjusting the EDF lengths, e.g. as shown in Fig. 2, at a pump power of 50mW, a DPB SFS could be operated in a zero slope region as the EDF length was 10m, and similarly for an 11m long EDF at 80mW pump. It is expected that the pump level at which $\partial \bar{\lambda}_{source}/\partial P_{pump} \simeq 0$ can be tuned over a wide range (at least 35–80mW limited by the lasers output power). Therefore, an SFS in the DPB configuration will exhibit stable mean wavelength operation with an appropriately chosen EDF length at high pump power.

Since a broader linewidth in an SFS implies that a higher SNR would be obtained if the SFS were to be used in an FOG [8], a large linewidth is therefore desirable for an Er-doped SFS. Fig. 3 depicts the linewidths of SFSs in both DPB and SPB configurations at various EDF lengths when pumped at 80mW. In the SPB configuration, the linewidths ranged from ~13 to 15nm when the EDF was > 10m, i.e. the SFS was in the saturated output power region. In contrast, in the DPB configuration, the linewidth increased from ~10 to 29nm as the length of EDF varied from 4–10nm. In the $\partial \bar{\lambda}_{source}/\partial P_{pump} = 0$ region, i.e. at EDF length 11 m, the linewidth was ~27 nm These results indicate that a DPB SFS can provide not only a stable mean wavelength, but also broad linewidth operation. A higher SNR is therefore expected for an FOG system using such an SFS in the DPB configuration as a light source.

We also measured the pump efficiencies of SFSs in both DPB and SPB configurations. The SFSs consisted of 18m and 11m long EDFs in SPB and DPB configurations, respectively. The EDF lengths were chosen because of the considerations that a saturated output power could be obtained in an SPB configuration, and $\partial \bar{\lambda}_{source}/\partial P_{pump} \simeq 0$ operation could be attained at 80mW pump in

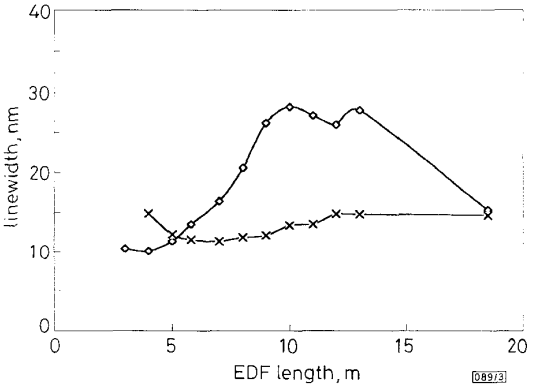

Fig. 3 *Linewidths of SFSs in both DPB and SPB configurations at various EDF lengths when pumped at 80mW*

—O— DPB
—×— SPB

the DPB configuration. The results indicate that a DPB SFS can provide a better pump efficiency (~22.6% against 13.3%) and larger output power (18.6 against 10.9mW) with a shorter EDF than an SPB SFS.

It should be noted that the optical feedback from the sensor loop experienced in an FOG may alter the characteristics of a DPB SFS. As the round trip gain of an SFS is > 1, the feedback may even cause lasing. Work is being directed towards characterising the feedback effects on the mean wavelength variation. Though an optical isolator is required, it is found that less isolation than in current usage may still be applicable to maintain the same results. Another important consideration is the effect of Er concentration in the current study. We have simulated such effects (Er: 80–200 mol ppm), and found that in general the aforementioned characteristics of an SFS in the DPB configuration still follow the same trends. More importantly, a pump-power insensitive mean wavelength operation with broad linewidth can still be achieved in the DPB configuration for various Er concentrations. Details will be reported elsewhere.

Conclusion: We have experimentally characterised, for the first time to our knowledge, an Er-doped superfluorescent fibre source pumped near 980nm in the double-pass backward configuration. The results indicate that its mean wavelength can be operated with little or no dependence on pump power when the length of EDF is properly chosen. Such pump-insensitive mean wavelength operation is vital to the light source utilised in a navigation-grade FOG. Additional advantages of an SFS in a DPB configuration over the commonly adopted single-pass backward configuration are broader linewidth and better pump efficiency when operating in stable mean wavelength regions.

22 July 1996
Electronics Letters Online No: 19961198

L.A. Wang and C.D. Chen (*Institute of Electro-Optical Engineering, National Taiwan University, Taipei, Taiwan, Republic of China*)

e-mail: lon@ccms.ntu.edu.tw

References

1 IWATSUKI, K.: 'Long-term bias stability of all PANDA fibre gyroscope with Er-doped superfluorescent fibre laser', *Electron. Lett.*, 1991, **27**, (12), pp. 1092–1093

2 DULING, I.N., MOELLER, R.P., BURNS, W.K., VILLARRUEL, C.A., GOLDBERG, L., SNITZER, E., and PO, H.: 'Output characteristics of diode pumped fibre ASE sources', *IEEE J. Quantum Electron.*, 1991, **QE-27**, (4), pp. 995–1003

3 WYSOCKI, P.F., DIGONNET, M.J.F., KIM, B.Y., and SHAW, H.J.: 'Characteristics of erbium-doped superfluorescent fibre sources for interferometric sensor applications', *J. Lightwave Technol.*, 1994, **LT-12**, (3), pp. 550–567

4 HALL, D.C., and BURNS, W.K.: 'Wavelength stability optimisation in Er-doped superfluorescent fibre sources', *Electron. Lett.*, 1994, **30**, (8), pp. 653–654

5 WYSOCKI, P.F., KALMAN, R.F., DIGONNET, M.J.F., and KIM, B.Y.: 'A comparison of 1.48μm and 980nm pumping for Er-doped superfluorescent fibre sources'. SPIE Fibre Laser Sources and Amplifiers III, 1991, **1581**, pp. 40–57
6 WYSOCKI, P.F., DIGONNET, M.J.F., and KIM, B.Y.: 'Wavelength stability of a high-output, brosadband, Er-doped superfluorescent fibre source pumped near 980 nm', *Opt. Lett.*, 1991, **16**, (12), pp. 961–963
7 HALL, D.C., BURNS, W.K., and MOELLER, R.P.: 'High-stability Er^{3+}-doped superfluorescent fibre sources', *J. Lightwave Technol.*, 1995, **LT-13**, (7), pp. 1452–1460
8 MORKEL, P.R., LAMING, R.I., and PAYNE, D.N.: 'Noise characteristics of high-power doped-fibre superluminescent sources', *Electron. Lett.*, 1990, **26**, (2), pp. 96–98

Low-loss coupling of 980nm GaAs laser to cleaved singlemode fibre

J.-M. Verdiell, M. Ziari and D.F. Welch

Indexing terms: Semiconductor junction lasers, Optical fibres, Optical couplers

The authors report the fabrication of 980nm wavelength lasers with reduced divergence angle and circular beams for high efficiency fibre coupling. Threshold currents of 50mA, singlemode output power of 70mW and <1dB coupling loss to a cleaved singlemode fibre are reported.

Introduction: Achieving efficient coupling of a laser diode beam to a singlemode fibre is an important goal in high power 980nm pump laser packaging. Singlemode fibre coupling of semiconductor lasers usually results in a very significant insertion loss of several decibels. This excess loss stems from the undesirable waveguide properties of laser diodes. Conventional semiconductor lasers support a highly divergent and elliptic mode with a small spot-size that does not match the mode size of singlemode fibres. The high beam divergence of semiconductor lasers in the vertical direction exceeds the acceptance angle (numerical aperture) of optical elements such as singlemode fibres and micro-lenses. The large numerical aperture in the perpendicular plane also causes large spherical aberrations in spherical lenses, such as ball lenses or lensed fibres, and results in large phase front distortion and additional coupling losses. Finally, the beam asymmetry of the laser beam, typically 3:1, seriously degrades the coupling efficiency into singlemode optical fibres with symmetric modes. In addition to the high coupling losses, the small laser waist size also translates into very tight alignment tolerances. Lasers with more symmetric circular beams and low vertical divergence angles could considerably improve packaging cost and performance. We report such a laser at 980nm that exhibits <1dB loss when coupled to a cleaved fibre.

Approach: The use of adiabatic tapers has been proposed to reduce the divergence of laser modes [1 – 8]. However, we chose to fabricate a large mode laser that does not rely on tapers, but solely on waveguide engineering. The advantage of this technique is a simpler fabrication process without a regrowth step, which would be difficult for 980nm lasers, due to the presence of Al on the overgrown layer. Mode shaping was obtained by adding thin extra layers of high Al-content, low index material on each side of the separate confinement heterostructure (SCH) of an otherwise conventional InGaAs quantum well laser design [9]. As a result, the effective index of the laser mode can be lowered to closely match that of the cladding layers by precisely adjusting the thickness of the low-index layer. When the difference between the modal effective index and the cladding layers index is small, the mode wings penetrate deeply into the cladding, resulting in an enlarged near-field spot and narrower far-field divergence. Additional high-index layers (GaAs layers) were also added deep into the cladding layers to promote modal stability against minute variations of the index of the SCH, which can be caused by carrier injection at high power levels. Fig. 1 shows the computed near-field mode intensity and the far-field pattern of the designed epitaxial structure, with a computed FWHM angle of 14°. The calculated $1/e^2$ width, which is a better measure of the divergence angle for packaging purposes, is only 23°.

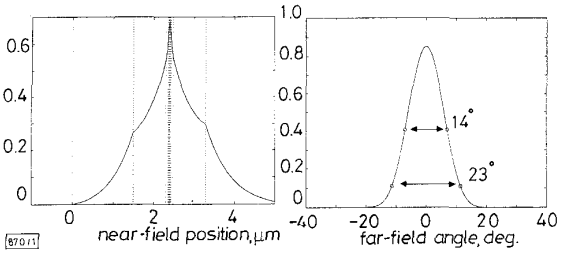

Fig. 1 *Computed mode profile and far field profile of low-divergence epitaxial structure at 980nm wavelength*

FWHM is 14°, with a $1/e^2$ width of ~23°

Experiments: Three wafers, differing only in the thickness of the low-index layers, were grown by MOCVD, and ridge lasers were processed. Low-index thicknesses of 150, 200 and 350Å were tried. As the thickness of the low-index layer increases, the modal index is expected to diminish, causing the mode to penetrate further into the cladding and the far-field divergence to decrease. This was confirmed by the experimental measurement shown in Fig. 2, which demonstrates that the far-field divergence perpendicular to the junction decreases progressively from 18.1 to 15.2°. For comparison, a similar structure without the low index layers had 28° divergence. Divergence in the plane of the junction was determined by the ridge structure and ranged from 8 to 11° due to process variations. As the low-index layer thickness increases, the threshold current also increases from 30 to 80mA, due to the diminution of the confinement factor, as shown on the L-I curves in Fig. 2. However, the differential efficiency is mostly unchanged and all lasers exceed 70mW output power CW. The ridge width was slightly wider than optimum, causing some light to be emitted in higher order lateral modes, with resulting small kinks in the L-I curve. The laser stayed perfectly singlemode in the transverse direction, in the whole operating range, which was our primary concern in this work. The wafer with an intermediate low-index layer thickness of 200A was the best compromise between narrow far-field and low threshold, and was used in the subsequent fibre coupling experiments. The measured far-field divergence at FWHM was 11.7 × 17.8°, (an aspect ratio of 1.5) with a 50mA threshold. The maximum output power was limited by thermal heating. A combination large cladding thickness, low *p*-doping in these unoptimised structures led to unusually high series resistance of over 10Ω, which was probably the cause of the thermal limitations in the *p*-up mount of the device.

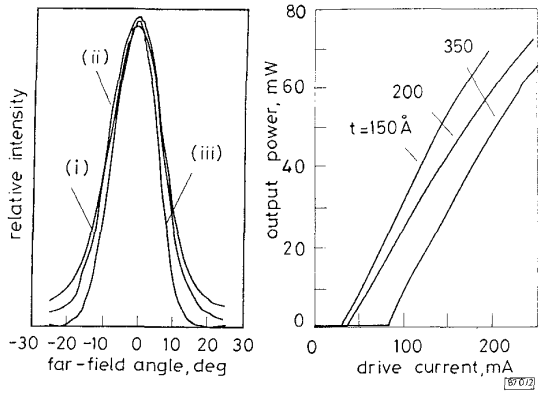

Fig. 2 *Far-field and L-I curves of three different 980nm laser structures with different thickness t of low-index layers*

Far-field angle narrows and threshold current increases with increasing layer thickness
(i) $\theta_i = 17.8°$, $t = 200$Å
(ii) $\theta_i = 18.1°$, $t = 150$Å
(iii) $\theta_i = 15.2°$, $t = 350$Å